Article

Noncytotoxic WORM Memory Using Lysozyme with Ultrahigh Stability for Transient and Sustainable Electronics Applications

Hritinava Banik, Surajit Sarkar, Debajyoti Bhattacharjee, Akshit Malhotra, Ashwini Chauhan, and Syed Arshad Hussain*

Cite This: *ACS Omega* 2024, 9, 618–627

Read Online

ACCESS | 📊 Metrics & More | 📰 Article Recommendations | SI Supporting Information

ABSTRACT: Biocompatibility and transient nature of electronic devices have been the matter of attention in recent times due to their immense potential for sustainable solutions toward hazardous e-wastes. In order to fulfill the requirement of high-density data-storage devices due to explosive growth in digital data, a resistive switching (RS)-based memory device could be the promising alternative to the present Si-based electronics. In this research work, we employed a biocompatible enzymatic protein lysozyme (Lyso) as the active layer to design a RS memory device having a device structure Au/Lyso/ITO. Interestingly the device showed transient, WORM memory behavior. It has been observed that the WORM memory performance of the device was very good with high memory window (2.78×10^2), data retention (up to 300 min), device yield (∼73.8%), read cyclability, as well as very high device stability (experimentally >700 days, extrapolated to 3000 days). Bias-induced charge trapping followed by conducting filament formation was the key behind such switching behavior. Transient behavior analysis showed that electronic as well as optical behaviors completely disappeared after 10 s dissolution of the device in luke warm water. Cytotoxicity of the as-prepared device was tested by challenging two environmentally derived bacteria, *S. aureus* and *P. aeruginosa*, and was found to have no biocidal effects. Hence, the device would cause no harm to the microbial flora when it is discarded. As a whole, this work suggests that Lyso-based WORM memory device could play a key role for the design of transient WORM memory device for sustainable electronic applications.
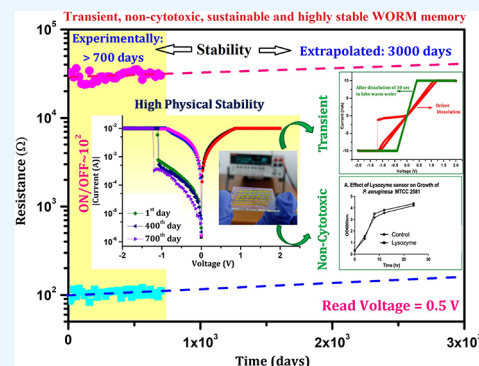
INTRODUCTION

Development of cloud computing, artificial intelligence, big data, Internet of Things (IoT), etc. requires exponential growth of memory devices due to their critical role toward contemporary computing systems.[1−4] The explosive growth of digital data triggers the urgent requirement of high-density data-storage devices. It has been predicted that the total available commercial semiconductor supply at present may not fulfill the memory device requirement by 2040.[5] On the other hand, most of the present electronic gadgets are made up of inorganic semiconductors as the basic element, which has physical limitation of downscaling.[3,6] Accordingly, conventional transistor memory may not fulfill the future high-density data-storage device requirement.[7] At the same time such materials develop hazardous impact on the environment leading to a huge amount of e-waste.[8,9] We are living in a technology-dependent society, where the life span of several electronic gadgets is very short. For example, the average life of smart phones and laptops are less than 4 years.[10] Some sensing devices, toys, and so forth have even shorter lifetimes of the order of few weeks, leading to a huge amount of e-waste generation.

Therefore, alternate solutions are highly desired to fulfill the high-density data-storage device requirement with a solution toward the e-waste issue. In this regard, resistive switching (RS)

memory employing environment friendly materials may be a potential alternative.[11,12] Unlike that of inorganic semiconductor-based memory, RS memory can be realized employing a variety of materials like organic, polymer, biocompatible, as well as green materials.[2,8,13,14] The features like low cost, down scalability, flexibility, low power consumption, high data density, as well as the simple device structure make RS devices more attractive toward memory applications.[6,14]

In RS memory, the resistance states of an insulating or dielectric material sandwiched between two electrodes can be switched between the high-resistance state (HRS) and the low-resistance state (LRS) upon application of electric bias.[1,11] Such a simple structure can be integrated on a large scale in a high-density data-storage system through the fabrication of a 3D cross-bar array structure.[15]

It is interesting to note that, several biocompatible as well as natural materials (plant extract) have already showed excellent

Table 1. WORM Memory Performances Employing Different Biomaterials

device configuration	threshold voltage (V)	memory window	retention time (s)	physical stability	transient nature	device yield (%)	refs
Ag/silk fibroin/Au	1.3–3.4	10^7–10^8	$\sim 10^4$				26
PEDOT:PSS/DNA/PEDOT:PSS	−2	10^4	$\sim 10^4$				27
Ag/albumen/ITO	2.2	2.0×10^7	1.1×10^5				28
Al/AuNP:lignin/Al	4.7	5×10^3	$\sim 10^3$				29
Al/CMS-GO/Al/SiO$_2$	2.22	10^5	$\sim 10^3$				30
Al/CNP:epoxy/Al	3	10^3–10^6					31
AgNW/PI(APAP)/DNAc	−1.4	10^4	$\sim 10^5$				32
Au/PS/ITO	1.33	4.57×10^3	$\sim 10^6$	210 days	8 min	87.5	33
Au/rose petal/ITO	1.1	1.23×10^2	7.2×10^3	~ 7 days			21
Au/Lyso/ITO	−0.96	2.8×10^2	1.8×10^4	700 days extrapolated up to 3000 days	10 s	73.8	present work

performance as RS devices.[16,17] A number of biomaterials, viz., proteins,[12] cellulose,[18] biopolymers,[19] polysaccharides,[20] natural plant extracts,[21] glucose,[22] chitosan,[23] and so forth, have been reported to show excellent RS behaviors with a wide variety of memory applications.[24] In addition to biocompatibility, biobased RS devices may be utilized to realize biorealistic synaptic devices for neuromorphic computation applications.[25] However, very few reports exist showing Write Once Read Many (WORM) applications employing biomaterials. A comparison of the WORM memory performance employing biomaterials based on the previously reported results has been listed in Table 1.

Despite having the potential to resolve the ever-increasing e-waste issues, biomaterial/biodegradable material-based RS devices have several concerns: (i) Mechanical stability as well as life span of electronic devices using biomaterials need to be improved; (ii) in order to reduce power consumption, a low threshold voltage is desired; (iii) transient nature at a faster rate is highly desired; and (iv) accurate deep theoretical knowledge explaining the conduction mechanism in the case of biomaterial-based RS devices is yet to be known.[15,16]

Therefore, high-performance RS devices showing WORM behavior using a variety of biomaterials are highly in demand. Also the stability of such devices must be taken care of. As a whole, the spectra of biocompatible materials under investigation need to be increased. Aiming at these issues, we have investigated the RS memory behavior employing an enzymatic protein lysozyme (Lyso) as the active layer. As far as literature survey is concerned, there exist very few reports of RS memory devices using enzymatic protein. Here, Lyso has been chosen due to its biocompatibility, regenerative nature, and easy availability. This can actually be found in egg white.[34] Presence of a large number of amino acids (~ 129) within the Lyso could be advantageous for the migration of charge carriers. Amino linkages and carboxylic groups present within the amino acids may act as potential trap centers for charge carriers.[33] Our investigations suggested Lyso may be used to design nonvolatile RS memory suitable for WORM memory applications. Interestingly, Lyso-based WORM memory device showed extra long stability, experimentally measured up to 700 days and extrapolated up to 3000 days. To the best of our knowledge, RS memory with such extra long stability has never been reported. Such a memory device also showed a transient nature, and the Lyso film could be completely dissolved into luke warm water within 10 s. Transient devices may be a suitable design of implantable electronics devices.[35] It has also been observed that Lyso-based RS device is noncytotoxic to environmental bacteria and potentially safe for environmental disposal.

EXPERIMENTAL SECTION

Materials and Methods. ITO-coated glass substrate of resistivity 15–25 Ω/Sq was procured from Sigma-Aldrich. Lysozyme was purchased from Sigma-Aldrich (purity >98%) and used as received without any further modification. Lysozyme solution was prepared by using ultrapure (18.2 MΩ cm, Milli-Q) distilled water with a concentration of 0.5 mg/mL. In order to record the field emission scanning electron microscopy (FESEM) image of the Lyso layer as well as the cross-sectional view of the device, a Sigma 300 microscope, Zeiss Pvt., Ltd. operated at a 5 kV acceleration voltage was employed. For spectroscopic studies, a UV–vis spectrophotometer from Shimadzu (UV-1800) was used. The materials and methods utilized for the cytotoxic studies are described in the Supporting Information.

Steps followed to carry out the work:

1. Lysozyme solution was prepared with concentration of 0.5 mg/mL in water.
2. To prepare the active layer of the device, Lyso solution was deposited onto ITO-coated glass substrate using a drop-casting method and kept overnight for drying.
3. Gold electrode was deposited onto the active layer using the sputtering technique to have the device with configuration Au/Lyso/ITO, where Au acts as the top electrode and ITO acts as the bottom electrode.
4. The device was then kept under vacuum followed by $I–V$ measurement using a source meter (Keithley − 2401) and a homemade/custom-made probe station.
5. Surface morphology of the active layer as well as the cross-sectional view of the Au/Lyso/ITO device was measured using a field emission scanning electron microscope at an acceleration voltage of 5 kV.
6. Transient nature of the device was investigated by exposing the device in normal distilled water bath and luke warm water bath followed by measuring the UV–vis absorption and $I–V$ curve as a function of time.
7. Cytotoxicity test of the as-prepared device was tested by challenging two environmentally derived bacteria *S. aureus* and *P. aeruginosa* followed by measuring the bacteria growth and viability.

RESULTS AND DISCUSSION

In order to have an idea about the surface morphology of the Lyso layer in the Au/Lyso/ITO device and the device structure, FESEM has been employed. FESEM image (Figure 1a) of the active layer (Lyso layer) of the device indicates that Lyso molecules are well distributed and organized throughout the
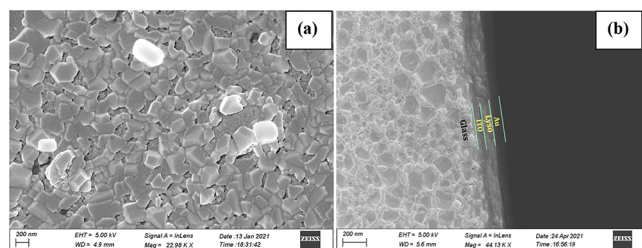
Figure 1. (a) FESEM image of the Lyso film drop-cast onto a clean glass slide and (b) cross-sectional FESEM image of the Au/Lyso/ITO device. The scale bar, accelerating voltage, as well as magnification during the FESEM measurement has been shown in the images.

active layer of the device. Surface morphology of the Lyso layer is in good agreement with the earlier reported results.[36] On the other hand, the cross-sectional FESEM image clearly depicts all three sections, that is, ITO (bottom electrode), Lyso (active layer), and gold (top electrode), in the device with marked distinctions. As a whole, FESEM studies confirm the successful formation of the Au/Lyso/ITO device.

Switching Behavior. In order to have an idea about the RS behavior, $I-V$ characteristics of the designed device (Au/Lyso/ITO) have been recorded by applying a voltage sweep in both positive and negative sweep directions. Corresponding $I-V$ curves are shown in Figure 2a,b, respectively, for initial positive and negative scan directions. Arrows in the figure indicate the sweep directions. Also the scan voltage sequences are mentioned in Figure 2a,b.

During the positive scan, initially the device is at its HRS, that is, OFF state where current is very less. At a certain voltage, the conducting state of the device changes, and it turns to a LRS, that is, ON state. This particular voltage is said to be the set voltage or popularly known as threshold voltage.[26] Here, the threshold voltage is 1.13 V. The operating speed is found to be 100 ns. Once the device is switched ON at 1.13 V, a reverse scan shows the high conducting nature of the device since it follows the linear relationship between current and voltage (Figure 2a). Interestingly, it has been observed that once the device is switched to its ON state (LRS), it retains the ON state, and HRS (OFF State) is never restored by applying the bias (scan) in either directions. It has also been observed that the device retains its ON (LRS) state even when the electrical power is switched OFF. That means the observed switching is irreversible

and nonvolatile in nature. RS devices with such behavior are suitable for WORM-type memory applications.[37] In such devices, the switching from HRS (OFF state) to LRS (ON state) may be considered as the writing in the memory devices. Once the information is written, the device stores it permanently and can be read many times.[38]

When the initial sweep direction is reversed, the device also showed almost similar WORM behavior with a negative threshold voltage $V_{Th}= -0.96$ V (Figure 2b). This indicates that the observed switching behavior for the Au/Lyso/ITO device is independent of the initial sweep direction. Idea about memory window (ON/OFF ratio) of such a memory device is obtained by comparing the resistances of the device in two states, that is, R_{HRS}/R_{LRS}, at a particular read voltage of 0.5 V[40]. Calculated memory window values for two initial sweep directions were of the order of 10^4 and 10^2, respectively, which are well within the acceptable value from application point of view as far as literature survey is concerned.[40] The memory window, the threshold voltage, as well as the device yield of the device for both initial scan directions are listed in Table 2.

Table 2. Illustration of Memory Performance Parameters in Both the Initial Positive and Negative Sweep Directions As Extracted from the $I-V$ curves Shown in Figure 2

initial sweep direction	memory window	threshold voltage (V_{Th})	standard deviation of V_{Th} (%)	device yield (%)
0 → +2 V	3.2×10^4	1.13 V	31.08	52.3
0 → −2 V	2.78×10^2	−0.96 V	9.2	73.8

A comparison with the previously reported results (Table 1) suggests that for biomaterial-based WORM devices, the threshold voltage observed in the present case is lower, which is advantageous in terms of lower power consumption.[41]

The device yield, that is, device reproducibility, has also been investigated for the Au/Lyso/ITO device for both the initial sweep directions. In order to do this, 84 independent switchable devices in two ITO-coated glass slides (7 × 6 arrays) have been prepared. All these 84 devices are almost similar structures with configuration Au/Lyso/ITO. Now 42 devices have been investigated applying initial scan in positive sweep direction and the remaining 42 devices by applying initial negative sweep direction. In the case of positive initial sweep, out of 42 devices,
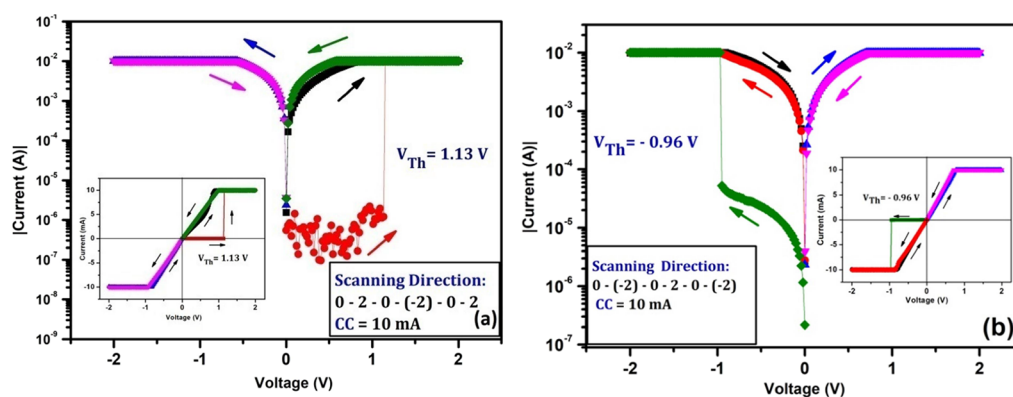
Figure 2. $I-V$ curve of the Au/Lyso/ITO device in semilog scale with voltage sweep $0-2-0-(-2)-0$ V keeping the compliance current at 10 mA. (b) $I-V$ curve of the Au/Lyso/ITO device in semilog scale with voltage sweep $0-(-2)-0-2-0$ V keeping the compliance current at 10 mA. Insets in (a) and (b) show the corresponding $I-V$ curves in linear scale for both sweep directions, respectively
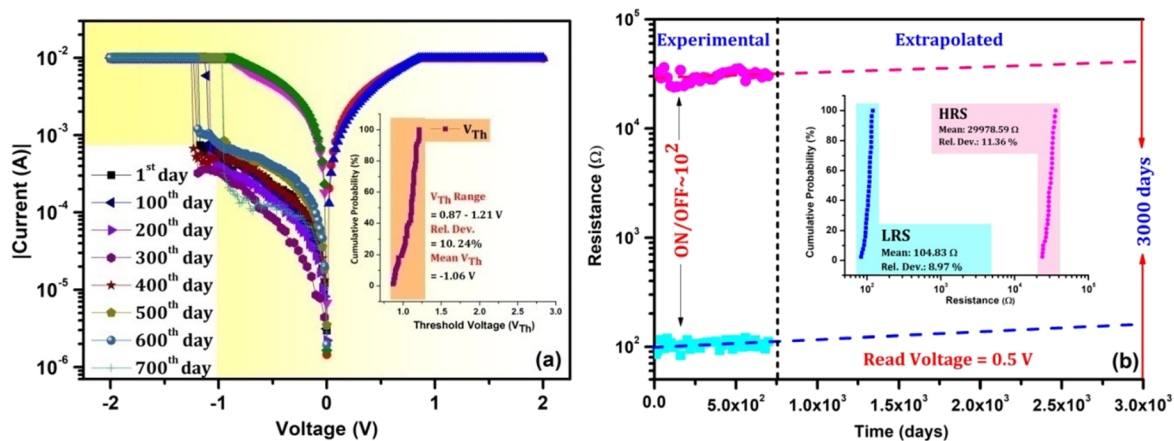
Figure 3. $I-V$ curves of the Au/Lyso/ITO device measured with the passage of time in semilog scale measured using sweep voltage $0-(-2)-0-2-0$ V and the compliance current 10 mA. (b) Plot of corresponding LRS and HRS resistance values along with the extrapolated curve (dotted) for LRS and HRS resistances up to 3000 days. Inset shows the cumulative probability with mean and relative deviation of V_{Th} (inset 3a) and LRS and HRS (inset 3b).
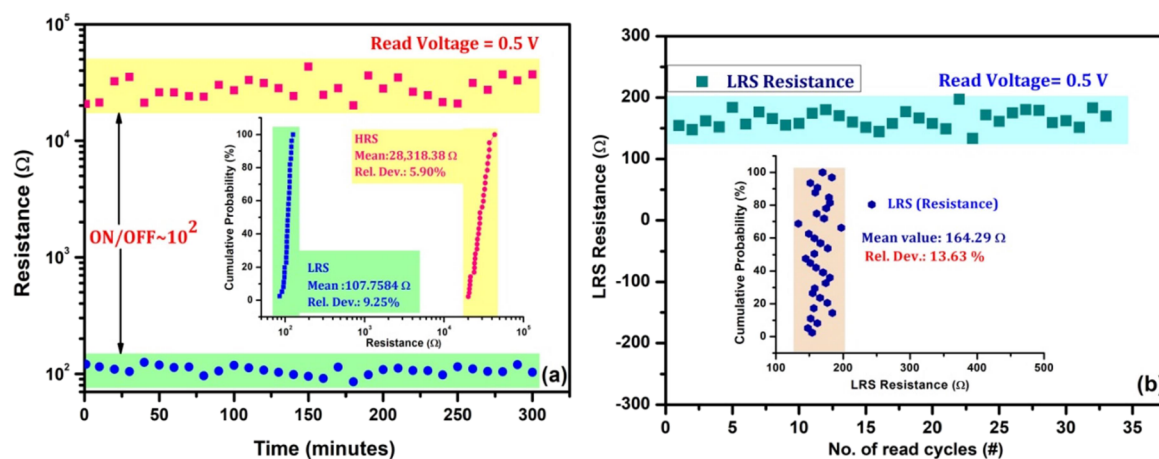
Figure 4. (a) Data retention characteristics of the device Au/Lyso/ITO at a read voltage of 0.5 V. Inset shows the plot of corresponding cumulative distribution of the LRS and HRS resistances. (b) Read cycles for the device Au/Lyso/ITO at read voltage of 0.5 V. Inset shows the plot of corresponding cumulative distribution of the LRS resistances.

22 devices showed reproducible WORM behavior with device yield 52.3%; on the other hand, for the initial negative sweep, out of 42 devices, 31 devices showed almost reproducible WORM behavior with device yield 73.8%. Information about device yield for the biomaterial-based WORM devices is hardly reported (Table 1), although information about device yield, that is, device reproducibility, is very crucial for real technological applications.[42] A device to device distribution of LRS and HRS resistances is shown in Figure S1 in the Supporting Information. From Table 2, it has been observed that the performance of the device with the initial negative sweep direction is better in terms of threshold voltage and device yield. RS device with lower threshold voltage is advantageous as it minimizes the power consumption requirement during write/read operation in the memory device.

Recent research trends suggest that RS-based memory devices have been considered as the promising candidate to replace Si-based memory devices.[1] In this regard, RS using biomaterials/biodegradable materials may have every potential to resolve the ever-increasing e-waste issues.[16] However, long-term stability of such devices is a serious concern in most of the cases.[16,17] For real practical applications, electronic device components must be stable for a certain period. In the present case, physical

stability of the Au/Lyso/ITO has been tested up to several months. In order to do that, a particular device was kept under ambient condition inside a sealed chamber to keep it away from any sort of contamination, dust, humidity, and so forth. $I-V$ characteristics of the device were measured with passage of time on a regular basis under ambient condition. It is very interesting to note that the device showed almost reproducible switching behavior even after 700 days from the day of device manufacture. The cumulative relative deviation of the threshold voltage/set voltage and the LRS resistance have been found to be 10.24% and 8.97%, respectively. The average values of LRS and HRS resistances are 104 Ω and 29.97 K Ω, respectively. Within the investigated period, the memory window degrades 29% with respect to freshly prepared device. Here, we checked the stability up to 700 days; however, even beyond that, the device was working. To the best of our knowledge, physical stability of RS devices using biomaterials for such a long period has never been reported. In the present WORM device, the read voltage is 0.5 V, and it has been observed that the memory window at this voltage even after 700 days hardly shows any significant degradation. In order to have an idea about the projected lifetime of the device beyond the tested period in terms of physical stability, an extrapolation method has been employed. It has been found that
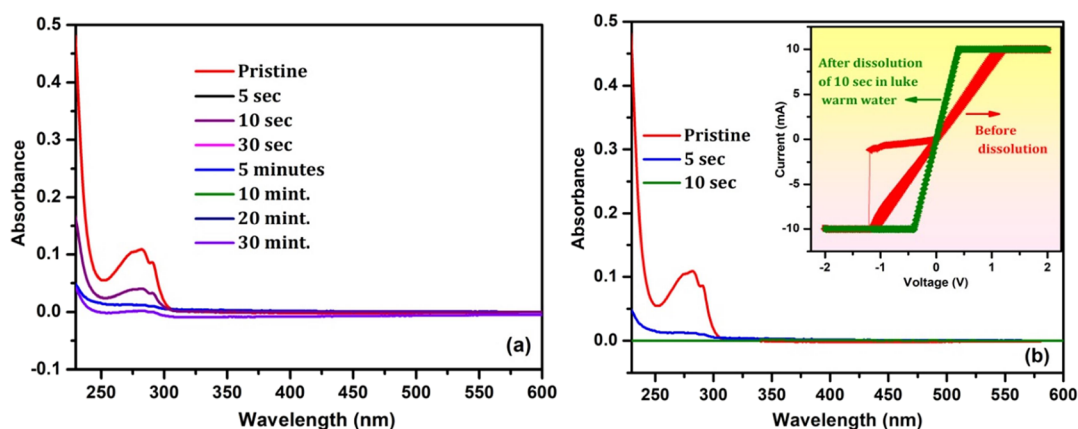
Figure 5. Absorption spectra of Lyso film with increasing dissolution time (a) in normal water and (b) luke warm water. $I-V$ curves of the device measured before dissolution and after 10 s of dissolution (in luke warm water) are shown in the inset of Figure 5b.

the WORM device made up of Lyso may be used even after 3000 days of manufacture with some variation in memory window as shown in Figure 3b. Based on the extrapolated results, it has been found that the memory window degrades up to 50% after 3000 days with memory window 245. As for the literature survey, this order of memory window is acceptable from application point of view.[40] Beyond this period, the memory window degrades at a faster rate and degradation becomes 75% after 3500 days and so on. Literature survey revealed that physical stability of biomaterial-based WORM devices is hardly reported (Table 1).[26,27,29]

In the case of memory devices, one of the important parameters is the data retention of the device. Retention time of the device is defined as the time up to which any state whether HRS or LRS is being retained once the device is switched OFF or ON, respectively.[43] This gives an idea about how long the device can retain the data/information written onto it. In order to do that, the designed Au/Lyso/ITO device has been switched to its LRS state, and LRS resistance has been continuously measured at the read voltage 0.5 V as shown in Figure 4a. Interestingly, it has been observed that the present WORM device can maintain its LRS ON state up to 300 min with negligible degradation in the memory window. LRS and HRS resistances were also found to be very stable with cumulative relative deviation of the order of 9.25% and 5.90%, respectively. Literature survey revealed that the data retention time ranges from 120 min to 3.6×10^4 minutes as reported by various authors in the case of biobased WORM devices (Table 1).[21,33] However, for real practical applications, data retention time needs to be increased further. It has been observed that by modifying the device fabrication like insertion of nanomaterials and other external agents, it is possible to enhance the data retention time.[44,45] An in-depth study is going on in our laboratory in this direction.

Read cycles of the designed Au/Lyso/ITO device have also been investigated. This gives the idea about the number of cycles of scan/sweep operation up to which a particular device gives reproducible results. In order to do that, initially the WORM device has been switched to its LRS state by applying the scan voltage $0 - (-2) - 0 - 2 - 0 - (-2)$ V for a particular device. After that, an exactly similar scan cycle has been applied to the same device at a regular interval. Interestingly, it has been observed that the device showed a reproducible ON state (conducting) behavior up to 33 consecutive scan cycles without significant degradation in the memory window. Plot of LRS

resistance at read voltage 0.5 V as a function of scan cycles is shown in Figure 4b. Cumulative probability distribution function indicates that the cumulative relative deviation in the LRS is 13. 63%.

Transient electronics is an emerging technology, where materials or devices disappear with minimal or nontraceable remains for a span of stable operation in a controlled fashion. It leaves environmentally and physiologically harmless byproducts in biofluids or in aqueous solutions.[35] In the present case, in order to check the transient nature of the device, we have performed the dissolution test in aqueous solution followed by spectroscopic as well as $I-V$ measurements. It has been observed that with the increase in dissolution time, the absorbance decreases. However, at ambient conditions, although the Lyso absorbance decreases, even after 30 min, it did not diminish completely (Figure 5a). Interestingly, when the same dissolution test is carried out with luke warm water, Lyso absorbance disappears immediately after only 10 s as shown in Figure 5b. This indicates the complete dissolution and transient nature of Lyso.

A similar test has also been done for the Au/Lyso/ITO device. Here, the whole device is dipped into luke warm water for 10 s, and then its $I-V$ characteristics have been measured with dissolution time. Corresponding curves are shown in the inset of Figure 5b. Here, the device initially showed WORM behavior. However, after 10 s of dissolution, the WORM behavior was completely lost, and the device showed ohmic behavior which resembles the characteristics of ITO.[46] As a whole, these investigations suggest that Lyso-based WORM memory device may be suitable for biodegradable transient electronics applications.

The enhancement of solubility of Lyso in luke warm water may be due to the enhancement in hydrogen bond length with temperature, It has been reported that the hydrogen bond length of water is affected by the temperature.[47] With the increase in temperature, the bond length increases leading to an increase in Lyso solubility.[48] Increase in Lyso solubility with temperature in aqueous solution has already been reported.[49] In the case of biobased WORM memory, hardly transient characteristics have been investigated (Table 1).[27,30,31] The observed transient characteristics are very good in terms of fast dissolution time even in comparison to the other type of RS memory or non-biobased resistive memory devices.[8]

In RS, typically a dielectric or insulator material changes its resistance states induced by an external electric bias.[6] It has been

proposed that different physical mechanisms and principles were involved in such RS behavior.[50] These may include redox reaction, ionic conduction, electron tunneling, hopping, space charge limited conduction, phase transition, and so forth.[43] In order to explore the conduction mechanism for the observed WORM behavior, the Au/Lyso/ITO devices as well as the $I–V$ curves were further analyzed.

UV–vis absorption spectra of the Lyso film shows a prominent band within 250–300 nm (Figure S2 of the Supporting Information).[51] Following Tauc's theorem, the energy band gap of the Lyso film has been extracted using the following equation

$$\alpha h\nu = A(h\nu - E_{\mathrm{g}})^{1/2} \quad (1)$$

where α is the optical absorption coefficient, $h\nu$ is the photon energy, A is the proportionality constant, and E_{g} is the optical energy band gap.[38] In the present case, the band gap for the Lyso film has been calculated from the intercept of the linear extrapolation of $(\alpha h\nu)^2$ vs $h\nu$ plot which is of the order of 4.97 eV (Figure S3 of the Supporting Information). This value lies well within the range of the band gap for insulator materials.[52]

In order to check the probability of metallic filament formation during the observed WORM memory behavior, $I–V$ curves of the Au/Lyso/ITO device have been measured at different temperatures ranging from 303 to 333 K. Reproducible switching behavior was observed at all temperatures. Interestingly, the plot of LRS resistance as a function of temperature revealed that the LRS resistances decrease with the increase in temperature (Figure S4 of the Supporting Information), whereas the LRS resistance increases with temperature when the metallic filament is formed.[53] This observation confirms that in the present case, the observed WORM behavior is not due to the conduction through metallic filament formation across the Lyso layer of the WORM device.[39]

Switching Mechanism. To explore the conduction mechanism further, $I–V$ curves of the present WORM device have been further analyzed following different standard theories.[54] Double logarithmic plot of the $I–V$ curves of the Au/Lyso/ITO device has been shown in Figure 6. Linear fitting of the curve revealed that at the low electric bias region of the HRS, the slope is ~1; this means the current is linearly proportional to the applied voltage which indicates that the device current follows ohmic behavior. The observed ohmic nature at the low bias region may be due to the thermally generated electrons within the active layer.[27] Here, the number of thermally generated electrons is higher than the injected electrons from the electrode and the conduction is governed by thermally generated electrons.[55] On the other hand, in the high bias region, a rapid increase in current is observed with slope ~2.30. This indicates that at the onset of switching, conduction through memory device obeys Child's law.[56] Hence, the current through the active layer is mainly due to the buildup of the charges injected from the source electrode and controlled by the trap centers existing within the active layer of the device.[55] These traps are filled up by the injected carriers. In such cases, the current density can be expressed as[57]
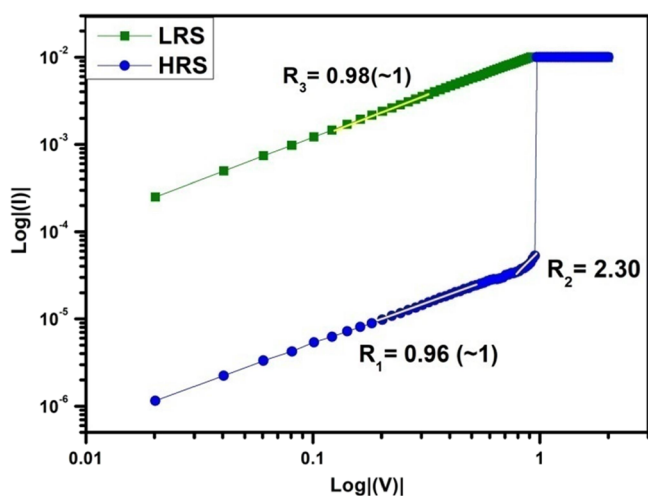
$$J = q^{1-l}\mu N\left(\frac{2l+1}{l+1}\right)^{l+1}\left(\frac{l}{l+1}\frac{\varepsilon_0\varepsilon_{\mathrm{r}}}{N_{\mathrm{t}}}\right)^l \frac{V^{l+1}}{d^{2l+1}} \quad (2)$$

where q is the elemental charge, l is the ratio of the characteristic temperature of the trap distribution to the operating temperature, μ is the carrier mobility, ε_{r} is the permittivity of the film, ε_{o} is the permittivity of free space, N_{t} is the trap density, N is the density of states in the conduction band or valence band, V is the applied voltage, and d is the film thickness.[57] Based on the depth of the trap centers, slight variations in the slope may also be observed.[27] In the present case, slope >2 indicates higher depth of the trap centers[46,58]. Trap-controlled SCLC involves the charge trapping-detrapping, which is consistent with Schottky emission.[55] This is also supported by the observed linear relationship of Ln I vs $V^{1/2}$ curve in the present case (Figure S5 of the Supporting Information). For the Au/Lyso/ITO WORM device, the trap centers may be due to the defects formed during Lyso film preparation.[59] It is well-known that the dielectric breakdown strength of thin films composed of biomolecules is extremely low, and the low dielectric breakdown strength may lead to higher defect density in the thin films.[59] Also, the chemical composition of Lyso molecules like the presence of carboxyl groups and amino linkages may form the trap centers as they act as the nucleophilic or electrophilic sites.[60] Typically, the traps are almost filled at the threshold voltage. Accordingly, a sharp rise in current is observed due to the further carrier injection. Here, the trap-controlled SCLC may be responsible for carrier transport mechanism ($I \propto V^2$).[27] On the other hand, at the LRS, the $I–V$ curve follows Ohm's law (scale ~1, $I \propto V$). This indicates the formation of conducting filament due to the injected electrons after the threshold voltage (V_{Th}).[58] In order to confirm the role of chemical composition of Lyso in the formation of traps, Au/Lyso/ITO devices have been exposed to 250 °C followed by $I–V$ measurement. Interestingly WORM behavior of the device has been lost completely. At 250 °C, all amino acids present in the Lyso molecule decomposed completely.[61] Accordingly, no traps were found, and the devices do lose the WORM behavior as shown in Figure S6 of the Supporting Information.

In order to further shed light on the conduction mechanism, the activation energy (E_a) for the Au/Lyso/ITO device has been calculated using the following equation[62]

$$I = I_0\exp\left(-\frac{E_{\mathrm{a}}}{KT}\right) \quad (3)$$

where K is the Boltzmann constant, E_{a} is the activation energy; T is the absolute temperature in K. Activation energy is defined as

Figure 6. Double logarithmic plot of the $I–V$ curve of the Au/Lyso/ITO device within the voltage scan range 0 − (−2) − 0 V.
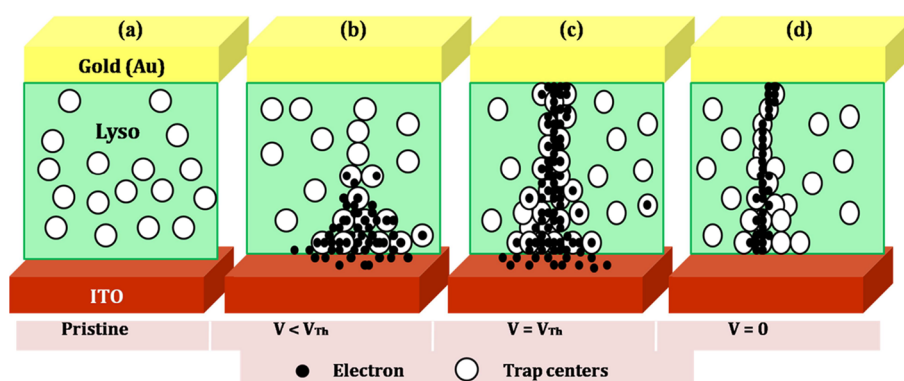
Figure 7. Schematic diagram of the charge transport mechanism across the active layer of the Au/Lyso/ITO WORM device. (a) Trap centers in the active layer under unbiased condition. (b) Injection of electrons and getting trapped inside the active layer when bias is applied and $V < V_{Th}$. (c) At $V = V_{Th}$, all traps within the active layer are filled up and a continuous conduction filament is formed in between the electrodes allowing flow of high current leading to LRS ON state. (d) Conduction filament remains intact even when the bias is withdrawn as the charge carriers are trapped inside the trap centers permanently. So, the device retains its ON state even in the absence of bias.

the energy difference between the transport level and the Fermi level in the case of organic semiconductor[63] or the energy difference between the trap state and the conduction band edge.[64] The slope at Ln (I/V) vs $1/KT$ gives the value of E_a.[65] (Figure S7 of the Supporting Information). The value of E_a is found to be 0.18 eV in the temperature region 303−333 K. In comparison to the optical energy band gap of Lyso (4.97 eV), the activation energy is very small. The small value of E_a in general indicates the existence of shallow traps or defects within the active layer of the device.[66] In the present case, the observed small value of E_a supports our earlier assumption about the existence of traps within the Lyso layer, and the observed switching is due to the trap-assisted conduction filament formation by SCLC.[66]

Interestingly, once the Au/Lyso/ITO device switches from HRS to LRS, the device remains permanently in that state showing WORM-like behavior.[67] This indicates that the detrapping or rupture of conducting filament did not occur even when the bias is removed.[68] A schematic diagram of the switching mechanism of the WORM device is shown in Figure 7. Also the device showed reproducible behavior up to several consecutive cycles with good read cycle. Physical stability of the device was also found to be very good. High cationic charge of the Lyso molecule may contribute to sustain the electron filament through strong electrostatic interaction between the electrons and charge-trapping sites, leading to better stability.[69] Also, there exists four disulfide bonds (S−S) and six helix regions within the Lyso molecule which provide high thermal stability.[70] Temperature dependence studies also supported this which revealed that the device showed reproducible WORM behavior up to 333 K.

In this work, we tried to demonstrate biocompatible RS memory devices. Toxicity is one of the major concerns at the time of disposal of electronic devices.[71] In order to assess the toxicity of our switch devices, we challenged Gram-positive (environmental isolate of *S. aureus*) and Gram-negative (environmental isolate of *P. aeruginosa*) bacteria with our device. Corresponding results are shown in Figure S8 of the Supporting Information along with the experimental procedure. The effect on the growth as well as the viability of these environmental isolates were evaluated. We observed that none of the isolates showed any changes in the growth patterns, as well as the cell viability, as determined after 24 h of treatment. The Lyso enzyme is specific to the cell wall structure of bacteria and is

not a broad spectrum for bacterial species.[72] Another key challenge for the Lyso enzyme is the evolution of bacterial resistance against the enzyme.[73] This memory device utilizes Lyso organic biomacromolecule to show excellent data-storage behavior besides being nonbiocidal to bacteria. Further, the biodegradable virtue of this RS memory device is enhanced by being non cytotoxic to environmental bacteria and potentially safe for environmental disposal with the least possibility to affect bacterial species present in the environment.

CONCLUSIONS

In summary, an RS memory device having the structure Au/Lyso/ITO has been prepared using an enzymatic protein Lyso as the active layer. The FESEM images as well as the absorption curve depict the presence of the Lyso layer in the device. Cross-sectional FESEM image gives visual information about the device structure with Au, Lyso, and ITO layer. The device demonstrated WORM memory behavior under an optimized electrical bias and compliance current. Memory window of the device was 10^2 and 10^4 for initial negative and positive sweep directions, respectively. Physical stability of the WORM memory device was tested experimentally for more than 700 days. Extrapolation of stability data indicated that the proposed WORM memory will give reliable performance even after 3000 days. Such a large period of stability is highly required for practical applications. The read cycle of the device is 33 cycles, and data retention is up to 300 min. Device yield was about 73.8%. The conduction mechanism mainly follows the Schottky emission of charge carriers in the HRS followed by the trap-controlled SCLC mechanism. Traps were inherent due to the chemical composition of the Lyso molecule or the defects formed during film formation. The designed WORM device showed a transient nature in luke warm water and completely vanishes with a dissolution time of 10 s. Cytotoxicity of the device has been characterized by challenging environmentally derived two kinds of bacteria and was found to have no inhibition. Hence, it does not have a biocidal activity upon exposure to the environment when discarded. As a whole, Lyso is being used to produce highly stable transient and sustainable WORM memory device which may have high potential toward the solution of e-waste.

■ ASSOCIATED CONTENT

Data Availability Statement

The data that supports the finding of this study are available in this article.

Ⓢ Supporting Information

The Supporting Information is available free of charge at https://pubs.acs.org/doi/10.1021/acsomega.3c06229.

Device to device distribution of LRS and HRS; absorption curve for the lysozyme; Tauc plot using the absorption curve for the lysozyme; variation of LRS current as a function of temperature; plot of $\ln(I)$ vs $V^{1/2}$ for the HRS for Schottky emission; $I-V$ curve of the device before and after exposure to 250 °C; ln (I/V) vs $1/KT$ curve; and cytotoxicity test (PDF)

■ AUTHOR INFORMATION

Corresponding Author

Syed Arshad Hussain − *Thin Film and Nanoscience Laboratory, Department of Physics, Tripura University, Suryamaninagar 799022 Tripura, India;* ⓞ orcid.org/0000-0002-3298-6260; Phone: +919402122510; Email: sahussain@tripurauniv.ac.in, sa_h153@hotmail.com; Fax: +913812374802

Authors

Hritinava Banik − *Thin Film and Nanoscience Laboratory, Department of Physics, Tripura University, Suryamaninagar 799022 Tripura, India*

Surajit Sarkar − *Thin Film and Nanoscience Laboratory, Department of Physics, Tripura University, Suryamaninagar 799022 Tripura, India*

Debajyoti Bhattacharjee − *Thin Film and Nanoscience Laboratory, Department of Physics, Tripura University, Suryamaninagar 799022 Tripura, India;* ⓞ orcid.org/0000-0003-2105-1889

Akshit Malhotra − *Department of Microbiology, Tripura University, Suryamaninagar, Tripura 799022, India*

Ashwini Chauhan − *Department of Microbiology, Tripura University, Suryamaninagar, Tripura 799022, India*

Complete contact information is available at:
https://pubs.acs.org/10.1021/acsomega.3c06229

Author Contributions

S.A.H. and H.B. designed the work. H.B., S.S., and A.M. performed all experiments and data analysis. S.A.H. and H.B. wrote the manuscript with input from A.C. and D.B.

Notes

The authors declare no competing financial interest.

■ ACKNOWLEDGMENTS

■ REFERENCES

(1) Shi, T.; Wang, R.; Wu, Z.; Sun, Y.; An, J.; Liu, Q. A Review of Resistive Switching Devices: Performance Improvement, Characterization, and Applications. *Small Structures* **2021**, *2* (4), No. 2000109.

(2) Gao, S.; Yi, X.; Shang, J.; Liu, G.; Li, R.-W. Organic and Hybrid Resistive Switching Materials and Devices. *Chem. Soc. Rev.* **2019**, *48* (6), 1531−1565.

(3) Wang, Z.; Wu, H.; Burr, G. W.; Hwang, C. S.; Wang, K. L.; Xia, Q.; Yang, J. J. Resistive Switching Materials for Information Processing. *Nat. Rev. Mater.* **2020**, *5* (3), 173−195.

(4) Shi, Q.; Wang, J.; Aziz, I.; Lee, P. S. Stretchable and Wearable Resistive Switching Random-Access Memory. *Advanced Intelligent Systems* **2020**, *2* (7), No. 2000007.

(5) Lv, Z.; Wang, Y.; Chen, Z.; Sun, L.; Wang, J.; Chen, M.; Xu, Z.; Liao, Q.; Zhou, L.; Chen, X.; Li, J.; Zhou, K.; Zhou, Y.; Zeng, Y.-J.; Han, S.-T.; Roy, V. A. L. Phototunable Biomemory Based on Light-Mediated Charge Trap. *Advanced Science* **2018**, *5* (9), No. 1800714.

(6) Jeong, D. S.; Thomas, R.; Katiyar, R. S.; Scott, J. F.; Kohlstedt, H.; Petraru, A.; Hwang, C. S. Emerging Memories: Resistive Switching Mechanisms and Current Status. *Rep. Prog. Phys.* **2012**, *75* (7), No. 076502.

(7) Hilbert, M.; López, P. The World's Technological Capacity to Store, Communicate, and Compute Information. *Science* **2011**, *332* (6025), 60−65.

(8) Hu, W.; Yang, B.; Zhang, Y.; She, Y. Recent Progress in Physically Transient Resistive Switching Memory. *J. Mater. Chem. C* **2020**, *8* (42), 14695−14710.

(9) Liu, X.; Shi, M.; Luo, Y.; Zhou, L.; Loh, Z. R.; Oon, Z. J.; Lian, X.; Wan, X.; Chong, F. B. L.; Tong, Y. Degradable and Dissolvable Thin-Film Materials for the Applications of New-Generation Environmental-Friendly Electronic Devices. *Applied Sciences* **2020**, *10* (4), 1320.

(10) Polák, M.; Drápalová, L. Estimation of End of Life Mobile Phones Generation: The Case Study of the Czech Republic. *Waste Management* **2012**, *32* (8), 1583−1591.

(11) Raeis-Hosseini, N.; Lee, J.-S. Resistive Switching Memory Using Biomaterials. *J. Electroceram* **2017**, *39* (1), 223−238.

(12) Wang, H.; Meng, F.; Zhu, B.; Leow, W. R.; Liu, Y.; Chen, X. Resistive Switching Memory Devices Based on Proteins. *Adv. Mater.* **2015**, *27* (46), 7670−7676.

(13) Qi, Y.; Sun, B.; Fu, G.; Li, T.; Zhu, S.; Zheng, L.; Mao, S.; Kan, X.; Lei, M.; Chen, Y. A Nonvolatile Organic Resistive Switching Memory Based on Lotus Leaves. *Chem. Phys.* **2019**, *516*, 168−174.

(14) Rahman, F. Y.; Bhattacharjee, D.; Hussain, S. A. An Account of Natural Material-Based Nonvolatile Memory Device. *Proc. Natl. Acad. Sci., India, Sect. A Phys. Sci.* **2023**, *93*, 497.

(15) Seok, J. Y.; Song, S. J.; Yoon, J. H.; Yoon, K. J.; Park, T. H.; Kwon, D. E.; Lim, H.; Kim, G. H.; Jeong, D. S.; Hwang, C. S. A Review of Three-Dimensional Resistive Switching Cross-Bar Array Memories from the Integration and Materials Property Points of View. *Adv. Funct. Mater.* **2014**, *24* (34), 5316−5339.

(16) Rehman, M. M.; Ur Rehman, H. M. M.; Kim, W. Y.; Sherazi, S. S. H.; Rao, M. W.; Khan, M.; Muhammad, Z. Biomaterial-Based Nonvolatile Resistive Memory Devices toward Ecofriendliness and Biocompatibility. *ACS Appl. Electron. Mater.* **2021**, *3* (7), 2832−2861.

(17) Cheong, K. Y.; Tayeb, I. A.; Zhao, F.; Abdullah, J. M. Review on Resistive Switching Mechanisms of Bio-Organic Thin Film for Non-Volatile Memory Application. *Nanotechnol. Rev.* **2021**, *10* (1), 680−709.

(18) Rananavare, A. P.; Kadam, S. J.; Prabhu, S. V.; Chavan, S. S.; Anbhule, P. V.; Dongale, T. D. Organic Non-Volatile Memory Device Based on Cellulose Fibers. *Mater. Lett.* **2018**, *232*, 99−102.

(19) Raeis-Hosseini, N.; Lee, J.-S. Controlling the Resistive Switching Behavior in Starch-Based Flexible Biomemristors. *ACS Appl. Mater. Interfaces* **2016**, *8* (11), 7326−7332.

(20) Lim, Z. X.; Cheong, K. Y. Nonvolatile Memory Device Based on Bipolar and Unipolar Resistive Switching in Bio-Organic Aloe Polysaccharides Thin Film. *Advanced Materials Technologies* **2018**, *3* (5), No. 1800007.

(21) Yasmin Rahman, F.; Sarkar, S.; Banik, H.; Jashim Uddin, Md.; Bhattacharjee, D.; Arshad Hussain, S. Investigation of Non Volatile Resistive Switching Behaviour Using Rose Petal. *Materials Today: Proceedings* **2022**, *65*, 2693−2697.

(22) Park, S. P.; Tak, Y. J.; Kim, H. J.; Lee, J. H.; Yoo, H.; Kim, H. J. Analysis of the Bipolar Resistive Switching Behavior of a Biocompatible Glucose Film for Resistive Random Access Memory. *Adv. Mater.* **2018**, *30* (26), No. 1800722.

(23) Hosseini, N. R.; Lee, J.-S. Biocompatible and Flexible Chitosan-Based Resistive Switching Memory with Magnesium Electrodes. *Adv. Funct. Mater.* **2015**, *25* (35), 5586−5592.

(24) Banik, H.; Sarkar, S.; Yasmin Rahman, F.; Kalita, H.; Bhattacharjee, D.; Arshad Hussain, S. RRAM and WORM Memory Devices Using Protamine Sulfate and Graphene Oxide. *Materials Today: Proceedings* **2022**, *65*, 2773−2777.

(25) Lv, Z.; Zhou, Y.; Han, S.-T.; Roy, V. A. L. From Biomaterial-Based Data Storage to Bio-Inspired Artificial Synapse. *Mater. Today* **2018**, *21* (5), 537−552.

(26) Wang, H.; Du, Y.; Li, Y.; Zhu, B.; Leow, W. R.; Li, Y.; Pan, J.; Wu, T.; Chen, X. Configurable Resistive Switching between Memory and Threshold Characteristics for Protein-Based Devices. *Adv. Funct. Mater.* **2015**, *25* (25), 3825−3831.

(27) Lam, J.-Y.; Jang, G.-W.; Huang, C.-J.; Tung, S.-H.; Chen, W.-C. Environmentally Friendly Resistive Switching Memory Devices with DNA as the Active Layer and Bio-Based Polyethylene Furanoate as the Substrate. *ACS Sustainable Chem. Eng.* **2020**, *8* (13), 5100−5106.

(28) Qu, B.; Lin, Q.; Wan, T.; Du, H.; Chen, N.; Lin, X.; Chu, D. Transparent and Flexible Write-Once-Read-Many (WORM) Memory Device Based on Egg Albumen. *J. Phys. D: Appl. Phys.* **2017**, *50* (31), 315105.

(29) Wu, W.; Han, S.-T.; Venkatesh, S.; Sun, Q.; Peng, H.; Zhou, Y.; Yeung, C.; Li, R. K. Y.; Roy, V. A. L. Biodegradable Skin-Inspired Nonvolatile Resistive Switching Memory Based on Gold Nanoparticles Embedded Alkali Lignin. *Org. Electron.* **2018**, *59*, 382−388.

(30) Liu, T.; Wu, W.; Liao, K.-N.; Sun, Q.; Gong, X.; Roy, V. A. L.; Yu, Z.-Z.; Li, R. K. Y. Fabrication of Carboxymethyl Cellulose and Graphene Oxide Bio-Nanocomposites for Flexible Nonvolatile Resistive Switching Memory Devices. *Carbohydr. Polym.* **2019**, *214*, 213−220.

(31) Hattenhauer, I.; Radomski, F. A. D.; de Araujo Duarte, C.; Mamo, M. A. Epoxy Resin in Organic WORM Memories: From Capsuling to the Active Layer. *Org. Electron.* **2016**, *34*, 57−66.

(32) Shih, C.-C.; Chung, C.-Y.; Lam, J.-Y.; Wu, H.-C.; Morimitsu, Y.; Matsuno, H.; Tanaka, K.; Chen, W.-C. Transparent Deoxyribonucleic Acid Substrate with High Mechanical Strength for Flexible and Biocompatible Organic Resistive Memory Devices. *Chem. Commun.* **2016**, *52* (92), 13463−13466.

(33) Banik, H.; Sarkar, S.; Bhattacharjee, D.; Hussain, S. A. Transient WORM Memory Device Using Biocompatible Protamine Sulfate with Very High Data Retention and Stability. *ACS Appl. Electron. Mater.* **2021**, *3* (12), 5248−5256.

(34) Shahmohammadi, A. Lysozyme Separation from Chicken Egg White: A Review. *Eur. Food Res. Technol.* **2018**, *244* (4), 577−593.

(35) Wang, H.; Zhu, B.; Ma, X.; Hao, Y.; Chen, X. Physically Transient Resistive Switching Memory Based on Silk Protein. *Small* **2016**, *12* (20), 2715−2719.

(36) Hekmat, D.; Hebel, D.; Joswig, S.; Schmidt, M.; Weuster-Botz, D. Advanced Protein Crystallization Using Water-Soluble Ionic Liquids as Crystallization Additives. *Biotechnol. Lett.* **2007**, *29* (11), 1703−1711.

(37) Sun, Y.; Wen, D. Nonvolatile WORM and Rewritable Multifunctional Resistive Switching Memory Devices from Poly(4-Vinyl Phenol) and 2-Amino-5-Methyl-1,3,4-Thiadiazole Composite. *J. Alloys Compd.* **2019**, *806*, 215−226.

(38) Hsu, C.-C.; Tsai, J.-E.; Lin, Y.-S. A Write-Once-Read-Many-Times Memory Based on a Sol-Gel Derived Copper Oxide Semiconductor. *Physica B: Condensed Matter* **2019**, *562*, 20−25.

(39) Sarkar, S.; Banik, H.; Suklabaidya, S.; Deb, B.; Majumdar, S.; Paul, P. K.; Bhattacharjee, D.; Hussain, S. A. Resistive Switching of the Tetraindolyl Derivative in Ultrathin Films: A Potential Candidate for

Nonvolatile Memory Applications. *Langmuir* **2021**, *37* (15), 4449−4459.

(40) Zhou, J.; Cai, F.; Wang, Q.; Chen, B.; Gaba, S.; Lu, W. D. Very Low-Programming-Current RRAM With Self-Rectifying Characteristics. *IEEE Electron Device Lett.* **2016**, *37* (4), 404−407.

(41) Paul, R.; Banik, H.; Alzaid, M.; Bhattacharjee, D.; Hussain, S. A. Interaction of a Phospholipid and a Coagulating Protein: Potential Candidate for Bioelectronic Applications. *ACS Omega* **2022**, *7* (21), 17583−17592.

(42) Jo, S. H.; Lu, W. CMOS Compatible Nanoscale Nonvolatile Resistance Switching Memory. *Nano Lett.* **2008**, *8* (2), 392−397.

(43) Li, Y.; Long, S.; Liu, Q.; Lü, H.; Liu, S.; Liu, M. An Overview of Resistive Random Access Memory Devices. *Chin. Sci. Bull.* **2011**, *56* (28), 3072.

(44) Ko, Y.; Ryu, S. W.; Cho, J. Biomolecule Nanoparticle-Induced Nanocomposites with Resistive Switching Nonvolatile Memory Properties. *Appl. Surf. Sci.* **2016**, *368*, 36−43.

(45) Sarkar, S.; Banik, H.; Yasmin Rahman, F.; Majumdar, S.; Bhattacharjee, D.; Arshad Hussain, S. Effect of Long Chain Fatty Acids on the Memory Switching Behavior of Tetraindolyl Derivatives. *RSC Adv.* **2023**, *13* (38), 26330−26343.

(46) Dey, B.; Debnath, P.; Chakraborty, S.; Deb, B.; Bhattacharjee, D.; Majumdar, S.; Hussain, S. A. Study of Compression-Induced Supramolecular Nanostructures of an Imidazole Derivative by Langmuir−Blodgett Technique. *Langmuir* **2017**, *33* (34), 8383−8394.

(47) *Water's Hydrogen Bond Strength*; CRC Press: 2010; pp 87−104. DOI: 10.1201/EBK1439803561-10.

(48) Bokka, N.; Adepu, V.; Selamneni, V.; Sahatiya, P. Non-Contact, Controlled and Moisture Triggered Black Phosphorus Quantum Dots/PVA Film for Transient Electronics Applications. *Mater. Lett.* **2021**, *290*, No. 129477.

(49) Cacioppo, E.; Pusey, M. L. The Solubility of the Tetragonal Form of Hen Egg White Lysozyme from PH 4.0 to 5.4. *J. Cryst. Growth* **1991**, *114* (3), 286−292.

(50) Pan, F.; Chen, C.; Wang, Z.; Yang, Y.; Yang, J.; Zeng, F. Nonvolatile Resistive Switching Memories-Characteristics, Mechanisms and Challenges. *Progress in Natural Science: Materials International* **2010**, *20*, 1−15.

(51) Kato, A.; Tanimoto, S.; Muraki, Y.; Kobayashi, K.; Kumagai, I. Structural and Functional Properties of Hen Egg-White Lysozyme Deamidated by Protein Engineering. *Biosci., Biotechnol., Biochem.* **1992**, *56* (9), 1424−1428.

(52) Hybertsen, M. S.; Louie, S. G. Electron Correlation in Semiconductors and Insulators: Band Gaps and Quasiparticle Energies. *Phys. Rev. B* **1986**, *34* (8), 5390−5413.

(53) Gao, S.; Song, C.; Chen, C.; Zeng, F.; Pan, F. Dynamic Processes of Resistive Switching in Metallic Filament-Based Organic Memory Devices. *J. Phys. Chem. C* **2012**, *116* (33), 17955−17959.

(54) Padma, N.; Betty, C. A.; Samanta, S.; Nigam, A. Tunable Switching Characteristics of Low Operating Voltage Organic Bistable Memory Devices Based on Gold Nanoparticles and Copper Phthalocyanine Thin Films. *J. Phys. Chem. C* **2017**, *121* (10), 5768−5778.

(55) Ismail, M.; Rahmani, M. K.; Khan, S. A.; Choi, J.; Hussain, F.; Batool, Z.; Rana, A. M.; Lee, J.; Cho, H.; Kim, S. Effects of Gibbs Free Energy Difference and Oxygen Vacancies Distribution in a Bilayer ZnO/ZrO2 Structure for Applications to Bipolar Resistive Switching. *Appl. Surf. Sci.* **2019**, *498*, No. 143833.

(56) Mangalam, J.; Agarwal, S.; Resmi, A. N.; Sundararajan, M.; Jinesh, K. B. Resistive Switching in Polymethyl Methacrylate Thin Films. *Org. Electron.* **2016**, *29*, 33−38.

(57) Bharti, V.; Sharma, A.; Gupta, V.; Sharma, G. D.; Chand, S. Improved Hole Mobility and Suppressed Trap Density in Polymer-Polymer Dual Donor Based Highly Efficient Organic Solar Cells. *Appl. Phys. Lett.* **2016**, *108* (7), No. 073505.

(58) Sterin, N. S.; Nivedya, T.; Mal, S. S.; Das, P. P. Understanding the Coexistence of Two Bipolar Resistive Switching Modes with Opposite Polarity in CuxO ($1 \leq x \leq 2$)-Based Two-Terminal Devices. *J. Mater. Sci: Mater. Electron* **2022**, *33* (4), 2101−2115.

(59) Mukherjee, C.; Hota, M. K.; Naskar, D.; Kundu, S. C.; Maiti, C. K. Resistive Switching in Natural Silk Fibroin Protein-Based Bio-Memristors. *physica status solidi (a)* **2013**, *210* (9), 1797−1805.

(60) Sun, B.; Wei, L.; Li, H.; Jia, X.; Wu, J.; Chen, P. The DNA Strand Assisted Conductive Filament Mechanism for Improved Resistive Switching Memory. *J. Mater. Chem. C* **2015**, *3* (46), 12149−12155.

(61) Fujimaki, M.; Kato, H.; Hayase, F. Studies on Roasting Changes of Proteins: Part I. Changes of Casein and Lysozyme during Roasting. *Agric. Biol. Chem.* **1972**, *36* (3), 416−425.

(62) Ling, H.; Yi, M.; Nagai, M.; Xie, L.; Wang, L.; Hu, B.; Huang, W. Controllable Organic Resistive Switching Achieved by One-Step Integration of Cone-Shaped Contact. *Adv. Mater.* **2017**, *29* (35), No. 1701333.

(63) Barbot, A.; Lucas, B.; Di Bin, C.; Ratier, B. Cesium Carbonate-Doped 1,4,5,8-Naphthalene-Tetracarboxylic-Dianhydride Used as Efficient Electron Transport Material in Polymer Solar Cells. *Org. Electron.* **2014**, *15* (4), 858−863.

(64) Letizia, J. A.; Rivnay, J.; Facchetti, A.; Ratner, M. A.; Marks, T. J. Variable Temperature Mobility Analysis of N-Channel, p-Channel, and Ambipolar Organic Field-Effect Transistors. *Adv. Funct. Mater.* **2010**, *20* (1), 50−58.

(65) Zhou, G.; Duan, S.; Li, P.; Sun, B.; Wu, B.; Yao, Y.; Yang, X.; Han, J.; Wu, J.; Wang, G.; Liao, L.; Lin, C.; Hu, W.; Xu, C.; Liu, D.; Chen, T.; Chen, L.; Zhou, A.; Song, Q. Coexistence of Negative Differential Resistance and Resistive Switching Memory at Room Temperature in TiOx Modulated by Moisture. *Advanced Electronic Materials* **2018**, *4* (4), No. 1700567.

(66) Li, C.; Duan, L.; Li, H.; Qiu, Y. Universal Trap Effect in Carrier Transport of Disordered Organic Semiconductors: Transition from Shallow Trapping to Deep Trapping. *J. Phys. Chem. C* **2014**, *118* (20), 10651−10660.

(67) Hung, Y.-C.; Hsu, W.-T.; Lin, T.-Y.; Fruk, L. Photoinduced Write-Once Read-Many-Times Memory Device Based on DNA Biopolymer Nanocomposite. *Appl. Phys. Lett.* **2011**, *99* (25), 253301.

(68) Lim, S. L.; Li, N.-J.; Lu, J.-M.; Ling, Q.-D.; Zhu, C. X.; Kang, E.-T.; Neoh, K. G. Conductivity Switching and Electronic Memory Effect in Polymers with Pendant Azobenzene Chromophores. *ACS Appl. Mater. Interfaces* **2009**, *1* (1), 60−71.

(69) Show, P. L.; Ooi, C. W.; Song, C. P.; Chai, W. S.; Lin, G.-T.; Liu, B.-L.; Chang, Y.-K. Purification of Lysozyme from Chicken Egg White by High-Density Cation Exchange Adsorbents in Stirred Fluidized Bed Adsorption System. *Food Chem.* **2021**, *343*, No. 128543.

(70) Cegielska-Radziejewska, R.; Lesnierowski, G.; Kijowski, J. Properties and Application of Egg White Lysozyme and Its Modified Preparations - a Review. *Pol. J. Food Nutr. Sci.* **2008**, *58* (1), 5.

(71) Bakare, A. A.; Adeyemi, A. O.; Adeyemi, A.; Alabi, O. A.; Osibanjo, O. Cytogenotoxic Effects of Electronic Waste Leachate in Allium Cepa. *Caryologia* **2012**, *65* (2), 94−100.

(72) Hughey, V. L.; Johnson, E. A. Antimicrobial Activity of Lysozyme against Bacteria Involved in Food Spoilage and Food-Borne Disease. *Appl. Environ. Microbiol.* **1987**, *53* (9), 2165−2170.

(73) Ragland, S. A.; Criss, A. K. From Bacterial Killing to Immune Modulation: Recent Insights into the Functions of Lysozyme. *PLOS Pathogens* **2017**, *13* (9), No. e1006512.